Lumbar Vertebral Body Bone Microstructural Scaling in Small to Medium-Sized Strepsirhines

ROBERTO J. FAJARDO,[1]* JEREMY M. DESILVA,[2] RAJARAM K. MANOHARAN,[3] JAMES E. SCHMITZ,[1] LAURA M. MACLATCHY,[4] AND MARY L. BOUXSEIN[3]

[1]Department of Orthopaedics, University of Texas Health Science Center at San Antonio, San Antonio, Texas

[2]Department of Anthropology, Boston University, Boston, Massachusetts

[3]Center for Advanced Orthopaedic Studies, Beth Israel Deaconess Medical Center and Harvard Medical School, Boston, Massachusetts

[4]Department of Anthropology, University of Michigan, Ann Arbor, Michigan

ABSTRACT

Bone mass, architecture, and tissue mineral density contribute to bone strength. As body mass (BM) increases any one or combination of these properties could change to maintain structural integrity. To better understand the structural origins of vertebral fragility and gain insight into the mechanisms that govern bone adaptation, we conducted an integrative analysis of bone mass and microarchitecture in the last lumbar vertebral body from nine strepsirhine species, ranging in size from 42 g (*Microcebus rufus*) to 2,440 g (*Eulemur macaco*). Bone mass and architecture were assessed via μCT for the whole body and spherical volumes of interest (VOI). Allometric equations were estimated and compared with predictions for geometric scaling, assuming axial compression as the dominant loading regime. Bone mass, microarchitectural, and vertebral body geometric variables predominantly scaled isometrically. Among structural variables, the degree of anisotropy (Tb.DA) was the only parameter independent of BM and other trabecular architectural variables. Tb.DA was related to positional behavior. Orthograde primates had higher average Tb.DA (1.60) and more craniocaudally oriented trabeculae while lorisines had the lowest Tb.DA (1.25), as well as variably oriented trabeculae. Finally, lorisines had the highest ratio of trabecular bone volume to cortical shell volume (∼3x) and while there appears to be flexibility in this ratio, the total bone volume (trabecular + cortical) scales isometrically ($BM^{1.23}$, $r^2 = 0.93$) and appears tightly constrained. The common pattern of isometry in our measurements leaves open the question of how vertebral bodies in strepsirhine species compensate for increased BM. Anat Rec, 296:210–226, 2013. © 2013 Wiley Periodicals, Inc.

Key words: Strepsirhine; lumbar vertebra; allometry; trabecular bone; cortical bone; microCT

*Correspondence to: Roberto J. Fajardo, Ph.D., University of Texas Health Science Center at San Antonio, Department of Orthopaedics, MSC 7774, 7703 Floyd Curl Dr., San Antonio, TX 78213. Fax: 210-567-6295. E-mail: fajardor@uthscsa.edu

Received 4 September 2012; Accepted 16 October 2012.
DOI 10.1002/ar.22632
Published online 15 January 2013 in Wiley Online Library (wileyonlinelibrary.com).

INTRODUCTION

Strepsirhine primate body mass, positional behavior, and lumbar vertebral body morphology appear to be strongly correlated (Majoral et al., 1997; Shapiro and Simons, 2002; Shapiro, 2007). More recent reports suggest that strepsirhine lumbar vertebral body length and lumbar region length scale isometrically but positive allometry has also been reported for the lumbar region length (Majoral et al., 1997). Nevertheless, investigators have consistently noted that key morphological differences are found among strepsirhines with different trunk orientations and locomotor mode. Taxa whose torso is typically pronograde during postures and locomotion (i.e., arboreal quadrupeds) have relatively longer lumbar vertebral bodies and more lumbar vertebrae that contribute to increased stride length through flexion-extension of the torso (Shapiro and Simons, 2002). Orthograde taxa such as galagine vertical clingers and leapers also have relatively long lumbar vertebral bodies, but have fewer lumbar vertebrae so the lumbar region is relatively short, presumably to provide more stability in regular orthograde postures. Lorisines, which are considered "anti-pronograde" taxa, have relatively short lumbar regions presumably due to their highly variable movement patterns during slow climbing, underbranch and branch-bridging locomotion, and a concomitant need for more stiffness. In addition, the lorisine vertebral body has a relatively greater surface area (ventrodorsal and mediolateral increases) which is considered an adaptation to greater load transfer through the spine during anti-pronograde postures and locomotion (Shapiro, 2007).

The strepsirhine primate lumbar vertebral body, like those of other primates, is a short bone with a composite structure made of trabecular bone surrounded by a thin cortical shell. Experimental and computational studies using human vertebrae (Rockoff et al., 1969; McBroom et al., 1985; Yoganandan et al., 1988; Silva et al., 1997; Eswaran et al., 2006) have investigated the relative contributions of these two tissues to lumbar vertebral body strength in axial compression and found that the cortical shell carries up to 45% of compressive loads depending on the region (maximum load at middle third of craniocaudal length), indicating that the role of trabecular bone in vertebral body strength is primary (Silva et al., 1997; Eswaran et al., 2006; Fields et al., 2009). However, the cortical shell's contribution to strength may be greater if the associated trabecular bone is poorly organized (low anisotropy) (Silva et al., 1997) or if bending is the primary mode of loading (Fields et al., 2009). Although axial compression is likely to be the major mode of lumbar vertebral body loading across most species (Smit, 2002), bending loads will also occur. In humans, it is in this latter condition that the cortical shell's contribution to load bearing (e.g., Fields et al., 2009) may increase. The variety of positional behaviors among strepsirhines and other primates provides an opportunity to better understand the integrated function and mechanics of trabecular and cortical bone in lumbar vertebral bodies.

Body mass is an extremely important consideration in comparative studies of bone structure and mechanics. In general, joint forces should increase with increasing body mass, placing mechanical demands on the joint to increase in size or to alter the underlying bone mass, tissue density, or structure. In the lumbar vertebral body, adaptations to body mass could lead to several changes, including increased endplate cross-sectional area and/or changes in the trabecular or cortical bone relative volume, micro-architecture, or tissue density. For example, since trabecular bone may carry more of the load in lumbar vertebral body compressive loading, an increase in the vertebral body trabecular bone apparent density or bone volume fraction and the cross-sectional area would increase its compressive strength (Silva et al., 1997; Fields et al., 2009). Evidence indicates that vertebral body cross-sectional area scales isometrically (Shapiro and Simons, 2002) but no data exist regarding the scaling of strepsirhine trabecular bone volume fraction or any other architectural parameters. In contrast, data do exist for hominoids that indicate the cross-sectional area of the endplate, bone mass, and vertebral body length all increase isometrically with body mass in the eighth thoracic vertebral body whereas the trabecular bone volume fraction is invariant, trabecular thickness scales with negative allometry, and trabecular number scales with positive allometry as body mass increases (Cotter et al., 2009; Hernandez et al., 2009).

Beyond Cotter et al.'s (2009) work, few scaling studies have been published and the general impressions from trabecular bone studies suggest that scaling patterns are unclear. Patterns of trabecular bone scaling appear to depend on the anatomical site, taxa, and body mass range of the sample. Some studies of primate proximal femur trabeculae have suggested that Tb.Th is invariant with body mass (MacLatchy and Müller, 2002; Ryan and Ketcham, 2002; Fajardo et al., 2007b). In contrast, broad mammalian studies suggest that Tb.Th scales with negative allometry in the femur and humerus (Swartz et al., 1998; Doube et al., 2011). However, the Tb.Th scaling exponents are generally isometric for chiropteran proximal femora and humeri (Swartz et al., 1998), suggesting that within mammals scaling exponents may differ depending on the level of taxonomic resolution or locomotor behavior of the sample. Other data suggest that trabecular thickness increases sharply between mouse and pig or bovine but thickness increases are negligible between humans and elephants or whales (Mullender et al., 1996). In murine and human ontogeny, trabecular thickness and number positively correlate with age and body mass until body mass increases level off (Halloran et al., 2002; Glatt et al., 2007; Parsons et al., 2007; Gosman and Ketcham, 2009).

Here we report the results of a comparative study of strepsirhine primate last lumbar vertebral body microstructure, including trabecular bone and the cortical shell. We chose the last lumbar vertebral body because this ensured positional/anatomical homology across species with varying numbers of lumbar vertebrae (Shapiro et al., 2005). We investigated scaling trends in nine species that ranged 57-fold in body mass (42.5 g to 2,400 g) and included pronograde, orthograde, and anti-pronograde positional behavior groups (Shapiro and Simons, 2002; Shapiro, 2007). We tested the hypothesis that trabecular and cortical shell structure increase isometrically. As noted above, scaling exponents vary across studies, bones, and sample body mass ranges. The prediction of isometry is supported by that fact that lumbar vertebral body gross dimensions, such as

TABLE 1. Descriptions of the species sample, μCT voxel sizes, and diameters of the spherical volumes used with the Quant3D analytical software package

Species	Typical trunk orientation	Locomotor mode	n	Body mass[a] (g)	Voxel size[b] (mm)	Sph-VOI[c] (mm)
Microcebus rufus	Pronograde	Arboreal quadrupedalism	2	42.5	0.012	0.840 ± 0.204
Microcebus murinus	Pronograde	Arboreal quadrupedalism	4	61.0	0.012	0.858 ± 0.097
Galago senegalensis	Orthograde	Vertical clinging and leaping	5	282.0	0.020	1.080 ± 0.242
Cheirogaleus major	Pronograde	Arboreal quadrupedalism	4	438.0	0.020	2.493 ± 0.508
Lepilemur leucopus	Orthograde	Vertical clinging and leaping	2	605.5	0.030	1.590 ± 0.127
Nycticebus coucang	Anti-pronograde	Slow climbing, bridging, suspension	2	679.0	0.025	1.675 ± 0.177
Lepilemeur mustelinus	Orthograde	Vertical clinging and leaping	6	777.0	0.030	2.748 ± 0.130
Perodicticus potto	Anti-pronograde	Slow climbing, bridging, suspension	4	1250.0	0.020	2.733 ± 0.378
Eulemur macaco	Pronograde	Arboreal quadrupedalism	3	2440.0	0.036	3.816 ± 0.374

[a]Average species body masses were taken from Smith and Jungers (1997).
[b]Voxels are cubic.
[c]Average diameter of spherical VOI used in Quant3D microstructural analyses.

endplate cross-sectional area, vertebral body length, and lumbar region length scale with geometric similarity in strepsirhine primates as a group (Shapiro and Simons, 2002; Shapiro, 2007), even though trends differ between groups of strepsirhine primates (Shapiro and Simons, 2002). Furthermore, since our sample consists of mixed positional behavior groups it may cause an averaging of the individual scaling trends as is seen in the relationship of articular surface areas and body mass among anthropoid primates (Godfrey et al., 1991). Tests of dynamic strain similarity would be more appropriate in a study sample that consisted of a single, closely related positional behavior group, in particular terrestrial quadrupeds.

MATERIALS AND METHODS

The last lumbar vertebrae of nine adult strepsirhine primate species (n = 29) were used in this study. The sample consisted of species that ranged in body mass from 42.5 g (*Microcebus rufus*) to 2,440 g (*Eulemur macaco*) (Smith and Jungers, 1997). Included in this sample were orthograde (vertical-clinging and leaping), pronograde (quadrupedalism), and anti-pronograde taxa (branch-bridging, suspensory) (Table 1; Shapiro and Simons, 2002). Exclusion criteria for any specimen included clear signs of ankylosing spondylitis (and any other vertebral degenerative joint disease) or long bone fractures. Individuals were pooled within a species without regard to sex because several specimens lacked records and these species show little sexual size-dimorphism (Smith and Jungers, 1997). All materials were borrowed from the following museums: American Museum of Natural History (AMNH), the Museum of Comparative Zoology at Harvard University (MCZ), the Yale University Peabody Museum of Comparative Zoology (YPM) and the University of Zurich.

μCT Imaging

Volumetric X-ray images of the vertebrae were acquired with a μCT system (μ*CT*-40—Scanco Medical AG). Each vertebra was positioned in a cylindrical sample holder and secured using a synthetic foam mold. Scans were acquired in air with a 55 kV source, 114 μA current, 250 msec CCD camera exposure time, and 1,024×1,024 pixel matrix. The field of view was adjusted in each species to achieve the smallest cubic voxel dimensions. Voxel dimensions ranged between 12 μm^3 and 36 μm^3 (Table 1).

Two volumes of interest (VOIs) were created to characterize the whole vertebral body's (vb) (1) trabecular bone (Tb) and (2) cortical bone (Ct) shell using image analysis tools associated with the scanner. The protocol described below generally follows Fajardo et al. (2007a). Each μCT scan produced a three-dimensional stack that could be viewed slice by slice. Beginning 10 slices caudal to the last visual evidence of the cranial growth plate, we used a region of interest (ROI, which is a two-dimensional area) drawing tool to outline either the vertebral body's marrow cavity including all trabecular bone or the cortical bone shell. This process was repeated until a plane 10 slices cranial to the caudal growth plate was reached. The 10-slice buffer from both growth plates was chosen to avoid the transitional zone between the trabecular bone and the dramatically thinner and more abundant growth plate/endplate bone tissue. For the trabecular bone, ROI outlines followed the endosteal border of the vertebral centrum (Fig. 1a–c). A two-dimensional three pixel radial peel was applied to ensure that no cortical bone was included in the trabecular bone VOI. The cortical bone ROI was constructed by outlining the periosteal and endosteal boundaries of the cortical shell (Fig. 1d–f). At levels where the pedicles or transverse processes interrupted the cortical shell contiguity, the ROI was interrupted as well. The number of slices represented in each VOI ranged from 123 (*Galago senegalensis*) to 391 (*Perodicticus potto*) and the average was 252. In *M. rufus*, the species with the lowest body mass in the sample, the total height of the vertebral body VOI (vbVOI) was 2.4 mm or greater, which included virtually all the trabecular bone between the epiphyses. It is clear from three-dimensional images (Fig. 2) of the trabecular bone VOI that numerous trabeculae and inter-trabecular lengths (Harrigan et al., 1988) are sampled in this volume.

We also performed regional analyses of the cranial (cr) and caudal (ca) vertebral body trabecular bone using Quant3D (Ketcham and Ryan, 2004). Analyses were performed in spherical VOI centrally positioned on the images representing the 20th percentile and 80th percentile slices of the vbVOI (Fig. 1a–c). Once positioned, these spherical VOI were expanded until either the VOI

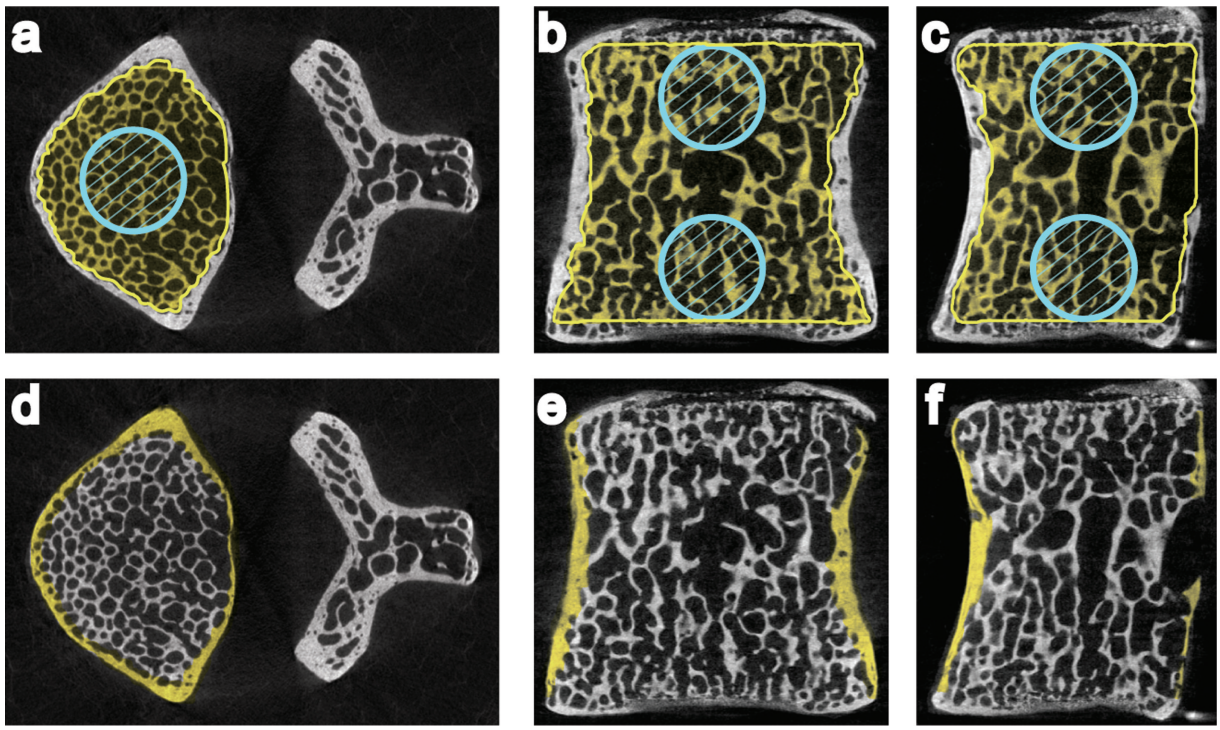

Fig. 1. Two-dimensional gray-scale images of a lorisine vertebra showing the various volumes of interest used in this study. The trabecular (**a–c**) and cortical (**d–f**) volumes of interest (VOI) for the whole body analyses are shown from axial (a, d), dorsoventral (b, e), and parasagittal (c, f) views. The trabecular bone spherical VOI (cranial, crVOI and caudal, caVOI) are also shown in these three perspectives (a–c). Methods for creating the VOI contoured to vertebral body follow the protocol described by Fajardo et al. (2007a).

boundary approached (1) a cortical bone endosteal border and/or (2) the cranial/caudal limits of the image slice stack. In general, the cortical bone boundary limited the VOI expansion in the smaller taxa and the image slice stack limited the VOI expansion in the larger taxa. In approximately 80% of the cases, this procedure successfully positioned the VOI within the endosteal boundary and at the stack limits (either cranial or caudal maximum). However, in cases where the VOI was within the endosteal boundary but not at the image stack limit (endplate boundary), the VOI was repositioned cranially/caudally to satisfy this criterion as well. All VOI excluded the most cranial and most caudal slice of the image stack. Table 1 lists the average spherical diameter per species. We sampled the cranial (crVOI) and caudal (caVOI) extremes of the vertebral body because these regions contain the greatest mass of trabecular bone and should carry the greatest fraction of the load. The sizes of these specimens, vertebral body morphologies (midheight narrowing), and our sampling protocol constrained our spherical VOI to less than 5 mm in diameter. In many cases, the volume sampled over three to five intertrabecular lengths (Harrigan et al., 1988), but it is best to consider that the continuum mechanics assumptions of trabecular bone may not apply well to these smaller VOI (Harrigan et al., 1988), unlike the case in the trabecular bone vbVOI.

We performed the spherical regional analyses for two reasons. First, previous work on humans indicates that trabecular architecture varies across and within vertebral bodies (Gong et al., 2005; Chen et al., 2008). Regional variation has never been investigated in strepsirhine primate vertebral bodies. Also, in light of concerns raised about measuring the degree of anisotropy in arbitrary volumes (Ketcham and Ryan, 2004; Gosman and Ketcham, 2009), we felt it important to perform another analysis that would provide an alternative view on the relationships between positional behavior and trabecular bone architecture. We measured BV/TV, Tb.Th, Tb.N, and the MIL-DA with the Quant3D method.

Trabecular bone VOI data (whole body and spherical VOI) were processed with an adaptive, iterative threshold (detailed in Ridler and Calvard, 1978; Trussell, 1979; Ryan and Ketcham, 2002; Meinel et al., 2005; Maga et al., 2006). In the vbVOI, the following three-dimensional trabecular bone structural and fabric properties (Table 2) were measured without any model assumptions (Parfitt et al., 1983; Guldberg et al., 2003) or concern for caveats related to measurements in two dimensional sections (i.e., stereology, Underwood, 1970; Weibel, 1979, 1980): trabecular bone volume (Tb.BV), trabecular bone volume fraction (Tb.BV/TV), structure model index (Tb.SMI) (Hildebrand and Ruegsegger, 1997a), trabecular number (Tb.N) (Hildebrand et al., 1999), trabecular thickness (Tb.Th) (Hildebrand and Rüegsegger, 1997b), trabecular separation (Tb.Sp) (Hildebrand et al., 1999), connectivity density (Tb.Conn.D), and the degree of anisotropy (Laib et al., 2000; Fajardo et al., 2007a). This degree of anisotropy (DA) method has been described previously (Laib et al., 2000; Fajardo et al., 2007a). In brief, this method uses the surface normal orientations from an object's triangulated surface mesh (hundreds to

thousands of points) to determine an orientation distribution. This distribution approximates the inverse of the mean intercept length (MIL) directional distribution and is subsequently fit to an ellipsoid using a least square approach. This approach has been used in the anthropological literature by several investigators, including most recently Shaw and Ryan (2012), DeSilva and Devlin (2012), and Wallace et al (2012). In the crVOI and caVOI we measured Tb.BV/TV, Tb.Th, and Tb.N. In all three VOI, the Tb.BV/TV was measured as the percentage of bone voxels to total VOI voxels after thresholding. In the spherical VOI, unlike the vbVOI, trabecular thickness and trabecular number were not measured using the standard distance transform methods (Hildebrand and Rüegsegger, 1997b; Hildebrand et al., 1999). Trabecular thickness, as previously described, was measured as the shortest intercept length at 1000 randomly positioned points in bone (Ryan and Krovitz, 2006; Gosman and Ketcham, 2009). Quant3D measures trabecular number as the number of intersections between the bone surface and a superimposed grid of lines normalized by the grid line length (Ryan and Krovitz, 2006; Gosman and Ketcham, 2009). Finally, the degree of anisotropy was measured in each spherical volume using Quant3D's mean intercept length module (Ketcham and Ryan, 2004). As already described, this module uses a directed secant sampling method to quantify the degree of anisotropy in three dimensions. We focused on the MIL(H)-DA technique so that anisotropies were all based on MIL-like protocols (vbVOI, crVOI, and caVOI). The settings for the MIL(H)-DA analyses were 513 uniform orientations with random rotations.

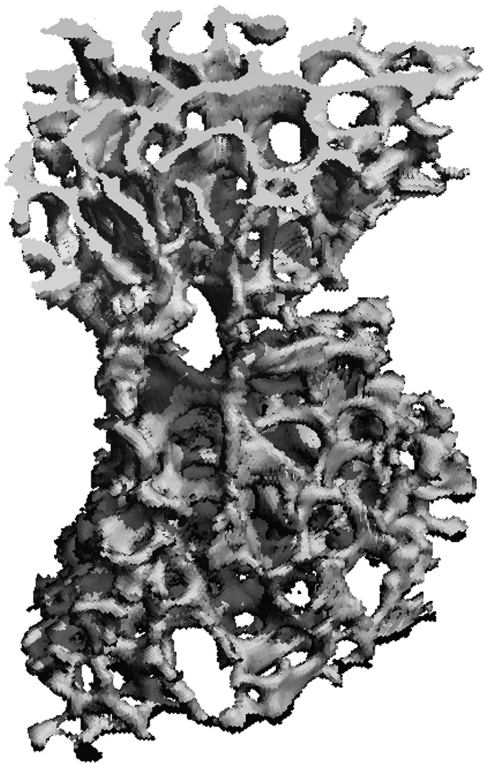

Fig. 2. Three-dimensional image of *M. rufus* trabecular bone. This vertebral body VOI (vbVOI) included all of the trabecular bone in the vertebral body between the cranial and caudal growth plates.

Cortical bone image data were processed using the threshold determined for vbVOI trabecular bone analyses. Cortical bone shell volume (Ct.BV) and thickness (Ct.Th) were measured in the cortical bone VOI after image processing.

Vertebral body cross-sectional area (CSA) was measured at a cranially positioned site in the vertebral body. It was measured on a single slice located caudal to the first slice in the vbVOI (cortical bone VOI always had the same height). The exact location was a distance 4% caudal to the most cranial slice of the vbVOI. This one slice protocol was implemented after a test on fourteen specimens indicated that vertebral body CSA showed negligible differences if measured on one, three, or six slices.

Vertebral Body Interspecific Allometry

We examined the relationship between body mass and the properties of the vertebral body to better understand how vertebral body size and microstructure scale as body mass increases interspecifically. These relationships were investigated in all VOI through correlation (e.g., dimensionless variables such as BV/TV) and regression methods using species means. We used

TABLE 2. Description of microstructural variables

Measurement	Abbreviation	Units	Description
Trabecular bone			
Bone volume	Tb.BV	mm^3	Volume of trabecular bone in the volume of interest
Bone volume fraction[a]	Tb.BV/TV	%	Ratio of bone volume to total volume of interest
Degree of anisotropy[a]	Tb.DA	(−)	Extent to which trabeculae are similarly oriented
Structure model index	Tb.SMI	(−)	Measure of distribution of rod- to plate-like trabeculae
Trabecular thickness[a]	Tb.Th	mm	Measure of average strut thickness
Trabecular separation	Tb.Sp	mm	Measure of average distance between struts
Trabecular number[a]	Tb.N	mm^{-1}	Measure of average number of trabeculae per millimeter
Connectivity density	Tb.Conn.D	mm^{-3}	Relative quantity describing how well are the struts interconnected
Cortical bone shell			
Cortical shell bone volume	Ct.BV	mm^3	Volume of cortical bone shell in the volume of interest
Cortical shell thickness	Ct.Th	mm	Measure of average cortical shell thickness
Body Area			
Cross-sectional area	CSA	mm^2	Measure of the total area of the vertebral body

[a]Parameters measured in whole vertebral body analyses and spherical VOI analyses.

published body masses for each species (Smith and Jungers, 1997) because samples were rarely associated with known body masses.

Data were log-transformed (natural log, Ln) and analyzed using a reduced major axis (Type II) model. We used the software SMATR (Warton and Weber, 2002; Warton et al., 2006) to perform these regression tests. We also used a phylogenetic generalized least squares (PGLS) approach to analyze the same data (Martins and Hansen, 1997) using the software COMPARE 4.6b (Martins and Hansen, 1997). We used species means and PGLS analyses to remain conservative in our approach, following recommendations by Nunn and Barton (2001). In addition, it has been reported that cortical bone properties carry a phylogenetic signal (O'Neill and Dobson, 2008). No similar study has been undertaken for trabecular bone tissue, but we chose to include phylogenetically-sensitive analyses to remain conservative in our approach rather than assume no influence of phylogeny. It is important to note that use of species means assumes negligible variation. We report the coefficients of variation along with other descriptive statistics to facilitate appreciation of intraspecific variation.

The phylogenetic information and branch lengths for the analysis were culled from several sources, including Yoder (2004), Chatterjee (2009), Seiffert et al. (2003), Seiffert (2007), Masters et al. (2007), Smith and Cheverud (2002), Matsui et al. (2009), and Purvis (1995). Our working phylogeny is reported in the Appendix in Newick notation. In addition, we performed ANCOVAs using SMATR to compare the vbVOI and spherical VOI results for Tb.BV/TV, Tb.DA, Tb.Th, and Tb.N. In these analyses, the natural log of body mass was the independent variable. We tested for common slopes across the three VOI and elevation shifts, if slopes were similar.

Confidence intervals of the slope were calculated in all regression tests. We compared the scaling exponent with the prediction for isometry. Clear statement of the assumed loading mode is important because it will impact the scaling predictions (Swartz et al., 1998). We assumed axial compression was the primary mode of loading in all taxa. Axial compressive loading is unlikely to be the only mode of loading, but evidence suggests that it is an important component of bipeds and quadrupeds (Smit, 2002). The isometry prediction value depends on the variable of interest and its dimensionality. For example, the trabecular bone volume fraction (Tb.BV/TV), a ratio of the bone volume to total volume, should be invariant with changes in body mass since trabecular bone volume (Tb.BV) and total volume should scale isometrically (BV $\propto M$, TV $\propto M$). For linear variables, such as the Tb.Th and Tb.N, the isometric predictions are $M^{1/3}$ (or a slope of 0.33 in log-log regression) and $M^{-1/3}$, respectively. The Tb.N expectation is negative because the total volume and distances between trabeculae are also absolutely increasing as body mass increases, thereby decreasing the linear density (number of trabeculae per millimeter) of the trabeculae as mass increases. The different isometry predictions for all variables are listed in Table 3.

Trabecular thickness and other measurements have been shown to be resolution dependent (Müller et al., 1996). Voxel sizes, in general, were larger for higher body mass species. As a result, trabecular thickness and other parameters could be correlated with body mass and voxel size. We calculated the partial and semipartial correlation coefficients to determine the strength of the relationship between Tb.Th and body mass when voxel size is controlled. Statistical significance of the partial correlation coefficient was determined using the F-statistic.

TABLE 3. Isometry predictions

Architectural parameter	Geometric similarity
Trabecular bone	
Tb.BV/TV	No correlation
Tb.SMI	No correlation
Tb.DA	No correlation
Tb.Th (mm)	$\propto M^{1/3}$
Tb.Sp (mm)	$\propto M^{1/3}$
Tb.N (mm^{-1})	$\propto M^{-1/3}$
Tb.Conn.D (mm^{-3})	$\propto M^{-1}$
Cortical bone	
Ct.Th (mm)	$\propto M^{1/3}$
Cross-sectional area	
CSA (mm^2)	$\propto M^{2/3}$

Mutual Associations of Trabecular Bone

Species means were used in analyses of the mutual associations of trabecular bone. We focused on two particular relationships. First, we examined the association between BV/TV and all other structural features, then between the DA and all other structural features. The focus was placed on these two parameters because they represent the relative quantity and fabric organization of the trabecular bone lattice, the two primary microarchitectural variables contributing to the strength and stiffness of trabecular bone (Turner et al., 1990; Turner, 1992). These relationships were analyzed interspecifically with parametric and non-parametric correlation tests.

RESULTS

Scaling

The descriptive statistics (mean, standard deviation, and coefficients of variation) are listed in Table 4. Coefficients of variation are not provided for the SMI since these values can be positive and negative in sign and will provide a misleading indication of variability.

Tb.BV/TV results were similar across all VOI and demonstrated an apparent nonlinear relationship with body mass whereby Tb.BV/TV increased as body mass (BM) increased through about 700 g in all VOI (Fig. 3a) but then plateaued. All Tb.BV/TV values peaked around the 500 to 750 g BM range but the crVOI Tb.BV/TV had a lower peak in this size range compared with the two other VOI. Parametric analyses indicated that the relationship between Tb.BV/TV and BM was significant in the crVOI but Tb.BV/TV was invariant in the other two VOI. The nonparametric correlation coefficients were significant in all three VOI (Table 5). The Tb.DA ranged between approximately 1.20 and 1.69 in the sample and was invariant with BM (Fig. 3b, Table 5). The orthograde primates generally had the highest Tb.DA values, the pronograde primates mid to high values, and the anti-pronograde lorisines consistently had the lowest Tb.DA values across all VOI. Higher DA values were

TABLE 4. Measurement means (standard deviation, coefficient of variation).

	M. rufus	*M. murinus*	*G. sengalensis*	*C. medius*	*L. leucopus*	*N. coucang*	*L. mustelinus*	*P. potto*	*E. macaco*
Tb.BV/TV (%)									
vbVOI	23.0 (3.4, 15%)	22.3 (3.0, 13%)	32.0 (3.7, 12%)	31.9 (2.3, 7%)	42.3 (2.0, 5%)	36.2 (6.8, 19%)	39.9 (3.9, 10%)	36.1 (2.3, 6%)	38.1 (0.1, 0.3%)
crVOI	23.2 (4.0, 17%)	23.3 (6.3, 27%)	29.7 (4.2, 14%)	30.4 (0.9, 3%)	38.6 (4.0, 10%)	33.0 (8.4, 25%)	36.4 (6.4, 18%)	35.6 (0.5, 1%)	37.9 (4.4, 12%)
caVOI	23.5 (4.3, 18%)	21.7 (6.0, 28%)	30.6 (5.8, 19%)	30.0 (2.4, 7%)	42.7 (3.2, 8%)	33.2 (7.1, 21%)	37.4 (5.2, 14%)	32.4 (1.8, 5%)	36.2 (1.2, 3%)
Tb.DA (1)									
vbVOI	1.50 (0.02, 1%)	1.63 (0.14, 9%)	1.69 (0.12, 7%)	1.36 (0.07, 5%)	1.56 (0.15, 10%)	1.27 (0.07, 6%)	1.53 (0.09, 6%)	1.24 (0.03, 2%)	1.43 (0.15, 11%)
crVOI	1.47 (0.10, 7%)	1.55 (0.27, 17%)	1.56 (0.08, 5%)	1.45 (0.10, 3%)	1.60 (0.33, 20%)	1.20 (0.08, 7%)	1.67 (0.14, 8%)	1.25 (0.04, 3%)	1.51 (0.01, 0.3%)
caVOI	1.48 (0.06, 4%)	1.44 (0.21, 15%)	1.55 (0.31, 20%)	1.44 (0.13, 11%)	1.61 (0.06, 4%)	1.24 (0.06, 5%)	1.60 (0.09, 6%)	1.24 (0.06, 5%)	1.49 (0.07, 5%)
Tb.Th (μm)									
vbVOI	54 (3, 5%)	59 (6, 9%)	100 (11, 11%)	98 (7, 7%)	150 (12, 8%)	120 (19, 16%)	145 (10, 7%)	135 (15, 11%)	218 (37, 17%)
crVOI	35 (1, 3%)	40 (7, 18%)	65 (10, 15%)	66 (9, 14%)	94 (9, 10%)	71 (14, 20%)	94 (8, 9%)	84 (8, 10%)	150 (29, 19%)
caVOI	35 (1, 4%)	36 (4, 11%)	61 (6, 10%)	62 (8, 15%)	90 (11, 12%)	73 (15, 21%)	89 (8, 9%)	75 (8, 10%)	144 (32, 27%)
Tb.N (mm^{-1})									
vbVOI	4.5 (0.4, 8%)	3.7 (0.4, 11%)	3.1 (0.4, 13%)	3.1 (0.4, 12%)	2.8 (0.3, 11%)	2.6 (0.4, 15%)	2.6 (0.3, 12%)	2.5 (0.2, 8%)	1.7 (0.2, 12%)
crVOI	5.5 (0.6, 12%)	4.7 (0.9, 20%)	3.5 (0.5, 13%)	3.9 (0.6, 9%)	2.8 (0.1, 4%)	3.9 (0.3, 8%)	3.1 (0.4, 14%)	3.6 (0.4, 11%)	2.0 (0.6, 30%)
caVOI	5.3 (0.1, 19%)	5.0 (0.7, 14%)	3.8 (0.4, 11%)	4.1 (0.7, 6%)	3.5 (0.4, 10%)	3.7 (0.1, 1%)	3.4 (0.4, 13%)	3.9 (0.4, 10%)	2.1 (0.6, 27%)
Tb.Sp (μm)									
vbVOI	210 (19, 9%)	263 (32, 12%)	322 (45, 14%)	302 (35, 12%)	341 (33, 10%)	311 (24, 8%)	365 (44, 12%)	379 (41, 11%)	603 (67, 11%)
Tb.Conn.D (mm^{-3})									
vbVOI	130.6 (28.0, 21%)	81.2 (29.4, 36%)	28.5 (4.5, 16%)	46.5 (14.7, 32%)	18.6 (12.5, 67%)	41.2 (1.4, 3%)	19.7 (4.4, 22%)	32.3 (11.3, 35%)	5.2 (1.0, 19%)
Tb.SMI (−)									
vbVOI	0.691 (0.148)	0.543 (0.269)	−0.289*(0.406)	−0.108 (0.199)	−1.097 (0.724)	−0.176 (0.535)	−1.024 (0.492)	−0.610 (0.425)	−0.963 (0.492)
Tb.BV (mm^3)									
vbVOI	0.837 (0.388, 46%)	1.240 (0.400, 32%)	2.687 (1.731, 64%)	29.012 (5.588, 19%)	10.504 (1.851, 18%)	27.589 (5.509, 20%)	47.947 (6.198, 13%)	66.335 (19.805, 30%)	105.833 (11.033, 10%)
Ct.Th (μm)									
vbVOI	80 (8, 10%)	90 (12, 13%)	158 (61, 38%)	165 (17, 10%)	265 (41, 16%)	176 (58, 33%)	258 (50, 19%)	205 (27, 13%)	456 (193, 42%)
Tb.BV/Ct.BV									
vbVOI	0.96 (0.26, 27%)	1.00 (0.16, 15%)	0.90 (0.22, 24%)	2.10 (0.36, 17%)	0.96 (0.12, 12%)	2.33 (0.47, 20%)	2.13 (0.59, 28%)	2.84 (0.27, 10%)	1.46 (1.03, 70%)
CSA (mm^2)									
vbVOI	2.700 (0.014, 0.5%)	3.638 (0.623, 17%)	4.216 (1.130, 27%)	21.420 (2.305, 11%)	13.705 (0.120, 0.9%)	23.744 (1.265, 5%)	31.022 (1.674, 5%)	35.295 (8.523, 24%)	63.367 (11.641, 18%)

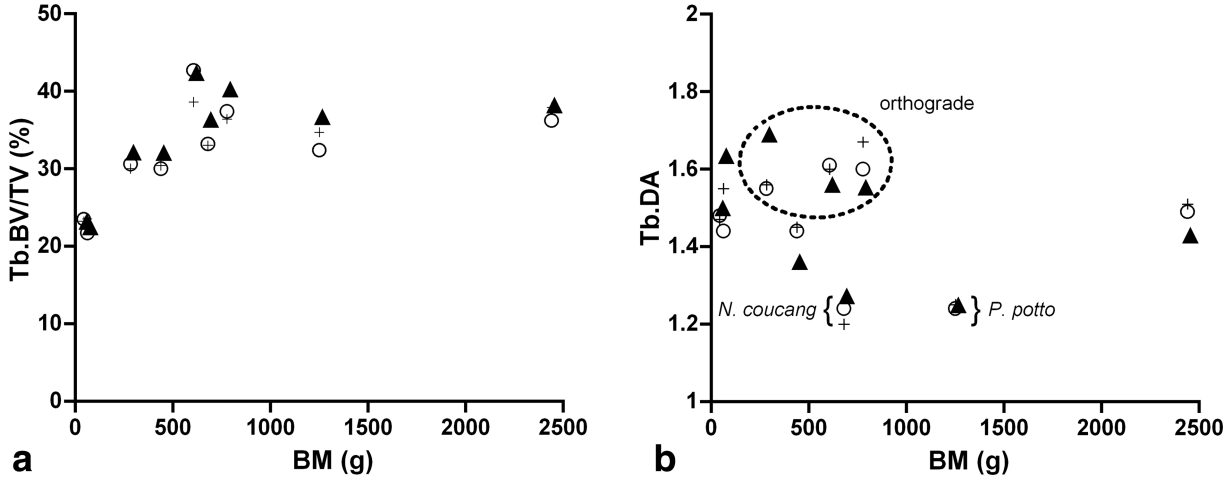

Fig. 3. Relationships between (**a**) trabecular bone volume fraction, the (**b**) degree of anisotropy and body mass (BM), in all trabecular bone VOI. A similar Tb.BV/TV pattern is observed in all three VOI. The Tb.BV/TV increases initially in all three VOI and then appears to plateau. The correlation between Tb.BV/TV and BM is significant only in the crVOI. The Tb.DA values are the highest in the vertical clinger and leapers. The lorisine species have the lowest anisotropy. Symbols: ▲, vbVOI, +, crVOI, ○, caVOI.

TABLE 5. Correlation tests values

	vbVOI		crVOI		caVOI	
	RMA/PGLS	*rho*	RMA/PGLS	*rho*	RMA/PGLS	*rho*
Tb.BV/TV	0.58/0.53	0.75*	0.70*/0.69*	0.82**	0.51/0.52	0.72*
Tb.DA	−0.41/−0.38	−0.53	−0.14/−0.02	−0.10	−0.12/−0.16	−0.03
Tb.SMI	−0.65/−0.66*	−0.72*	–	–	–	–

Parametric correlations were calculated using RMA and PGLS methods; nonparametric correlations were calculated using Spearman's [*rho*].
RMA, reduced major axis, PGLS, phylogenetic generalized least squares, whole vertebral body volume of interest (vbVOI), cranial spherical volume of interest (crVOI), caudal spherical volume of interest (caVOI), [*rho*], Spearman nonparametric correlation value.
*$P < 0.05$, **$P < 0.01$, see Table 2 for parameter abbreviations.

more closely associated with cranio-caudally oriented trabeculae in the last lumbar vertebrae (Fig. 4). The Tb.SMI showed a weak significantly decreasing association with BM (Table 5).

Tables 6 and 7 provide the results of the RMA and PGLS scaling analyses, respectively. Data are reported in two separate tables but it is important to note that the Model II and phylogenetic analytical approaches produce similar results. For example, Tb.Th increased isometrically (Tables 6 and 7, Fig. 5a) with BM across all the VOI. Although RMA scaling exponents were similar across the VOI (critical value: 0.003, $P = 1.0$), ANCOVA analyses (RMA) indicated that trabeculae were significantly thicker in the vbVOI ($F = 37.38$, $P > 0.001$) compared with the other two volumes of interest. Tb.N showed a similar pattern. The scaling exponents were similar in the three VOI (Tables 6 and 7, Fig. 5b) and centered around−0.20, which suggested that this parameter scaled with weak positive allometry since the expectation for isometry was−0.33. The only exception to this pattern was the result for the crVOI RMA, where the confidence limits included isometry. ANCOVA analysis on the RMA regressions indicated that the crVOI and caVOI regressions were significantly elevated relative to the vbVOI ($F = 10.129$, $P = 0.001$). Trabecular separation increased with slight negative allometry (Tables 6 and 7), most likely as a result of the positive allometry of Tb.N.

Body mass and voxel size correlated significantly with Tb.Th but the BM partial correlations were much higher than those for voxel size in all VOI (Table 8). The BM partial correlations were lower but remained significant when a subsample of specimens was analyzed but the voxel size partial correlations were not significant. Semi-partial correlations (not shown) were similar for BM but decreased for voxel size in all VOI.

Cortical shell thickness increased isometrically with BM (Tables 6 and 7), and showed only a weak negative trend with Tb.DA (Fig. 6). Vertebral body CSA, scaled isometrically as BM increased. The scaling exponent was high (>0.80), but the confidence limits of the slope were wide and included isometry (0.67, Tables 6 and 7).

The ratio of trabecular to cortical bone volume within the vbVOI varied between one and three (Table 4, Fig. 7a). Five of nine species invested equally in trabecular and cortical bone in the last lumbar vertebral body. These species included *M. rufus*, *M. murinus*, *G. senegalensis*, *L. leucopus*, and *E. macaco*. Approximately twice as much trabecular bone versus cortical bone was found in the vertebral bodies of *C. medius* and *L. mustelinus*. The two anti-pronograde lorisines, *N. coucang* and *P. potto* had the highest ratios of trabecular bone to

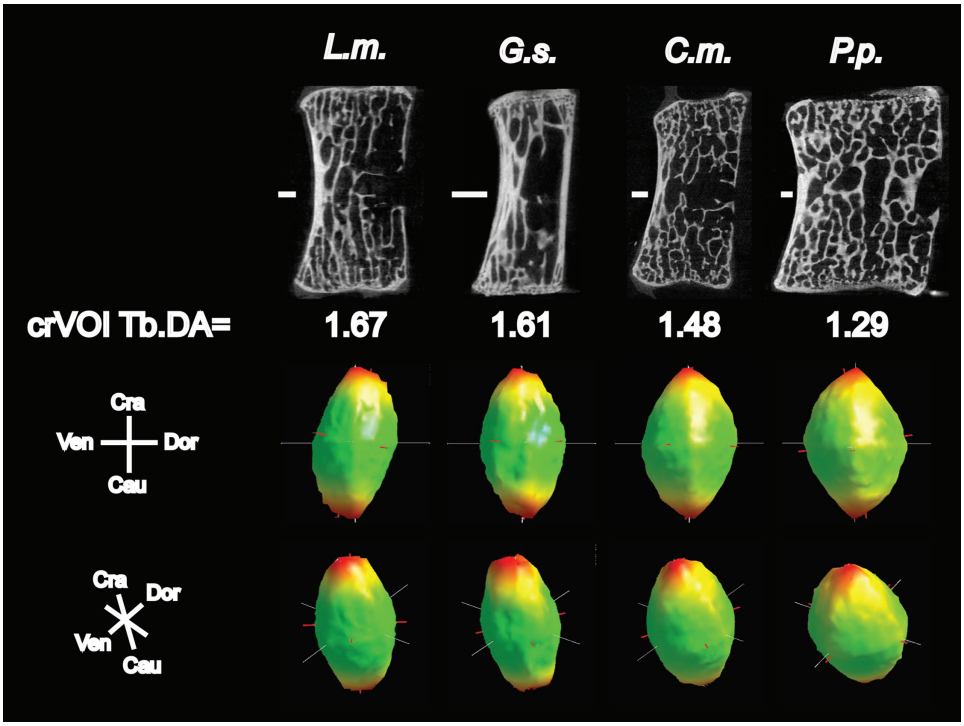

Fig. 4. Grey scale images (top row) showing parasagittal views of last lumbar vertebral trabecular and cortical bone, along with the Tb.DA results of the cranially positioned spherical VOI (crVOI). In these grey images, ventral is to the left of the image and dorsal to the right, cranial is toward the top of the page and caudal toward the bottom. Graphical representations (three-dimensional rose diagrams) of the anisotropy data produced by Quant3D are shown for two slightly different views. In the samples with high anisotropy, the clouds of data take on the shape of a narrow ellipsoids emphasizing the cranio-caudal orientations to the trabeculae. In the *P. potto*, the cranio-caudal orientation still predominates but the ellipsoid's fullness at its mid-substance suggests that other orientations in the mediolateral as well as dorsoventral directions are represented moreso than in species such as *L. mustelinus* and *G. senegalensis*. *L.m.*, *Lepilemur mustelinus*, *G.s.*, *Galago senegalensis*, *C.m.*, *Cheirogaleus major*, and *P.p.*, *Perodicticus potto*. Scale bars equal 0.5 mm.

TABLE 6. Results of reduced major axis allometric regressions

	df	r^2	*a*	*b*	CL	*P*	Trend
Trabecular bone							
Tb.Th							
vbVOI	7	0.93	2.7	0.33	0.27/0.42	<0.001	iso
crVOI	7	0.92	2.3	0.33	0.25/0.43	<0.001	iso
caVOI	7	0.90	2.2	0.33	0.25/0.44	<0.001	iso
Tb.N							
vbVOI	7	0.86	2.3	−0.21	−0.29/−0.15	<0.001	pos
crVOI	7	0.74	2.6	−0.22	−0.34/−0.14	<0.01	iso
caVOI	7	0.75	2.5	−0.20	−0.30/−0.13	<0.01	pos
Tb.Sp							
vbVOI	7	0.78	4.5	0.21	0.14/0.32	<0.01	neg
Tb.Conn.D							
vbVOI	7	0.77	7.6	−0.70	−1.06/−0.45	<0.01	iso
Cortical shell							
Ct.Th							
vbVOI	7	0.86	2.8	0.40	0.29/0.55	<0.001	iso
Cross-sectional area							
Cranial region	7	0.89	−2.4	0.84	0.63/1.13	<0.001	iso
Vertebral body total bone							
Ct.BV + Tb.BV	7	0.93	−4.3	1.23	0.98/1.55	<0.001	iso

df, degrees of freedom, *a*, *y*-intercept, *b*, regression slope, CL, confidence limits, *P*, probability, iso, isometry, pos, positive allometry, and neg, negative allometry. See Table 2 for other abbreviations. Significance results are of the test, H_0: slope (b) = 0.

cortical bone volume. When grouped by positional behavior, the anti-pronograde taxa (2.63 ± 0.41) were significantly higher than pronograde (1.39 ± 0.68, P = 0.0005) and orthograde taxa (1.43 ± 0.73, P = 0.0008). Log-scale scatterplots of Tb.BV and Ct.BV showed that trabecular bone investments increased as Ct.BV increased

TABLE 7. Results of phylogenetic generalized least squares allometric regressions.

	df	r^2	*a*	*b*	CL	*P*	Trend
Trabecular bone							
Tb.Th							
vbVOI	7	0.93	2.8	0.31	0.25/0.38	<0.001	iso
crVOI	7	0.91	2.4	0.31	0.24/0.38	<0.001	iso
caVOI	7	0.90	2.4	0.31	0.23/0.39	<0.001	iso
Tb.N							
vbVOI	7	0.85	2.3	−0.20	−0.26/−0.14	<0.01	pos
crVOI	7	0.70	2.4	−0.18	−0.27/−0.09	<0.05	pos
caVOI	7	0.72	2.4	−0.17	−0.25/−0.09	<0.05	pos
Tb.Sp							
vbVOI	7	0.75	4.6	0.19	0.11/0.28	<0.05	neg
Tb.Conn.D							
vbVOI	7	0.69	7.0	−0.58	−0.87/−0.30	<0.05	pos
Cortical shell							
Ct.Th							
vbVOI	7	0.85	3.0	0.36	0.25/0.47	<0.01	iso
Cross-sectional area							
Cranial region	7	0.93	−2.2	0.81	0.57/1.04	<0.001	iso
Vertebral body total bone							
Ct.BV + Tb.BV	7	0.91	−4.2	1.21	0.92/1.49	<0.001	iso

df, degrees of freedom, *a*, *y*-intercept, *b*, regression slope, CL, confidence limits, *P*, probability, iso, isometry, pos, positive allometry, and neg, negative allometry. See table 2 for other abbreviations significance results are of the test, H_0: slope (b) = 0.

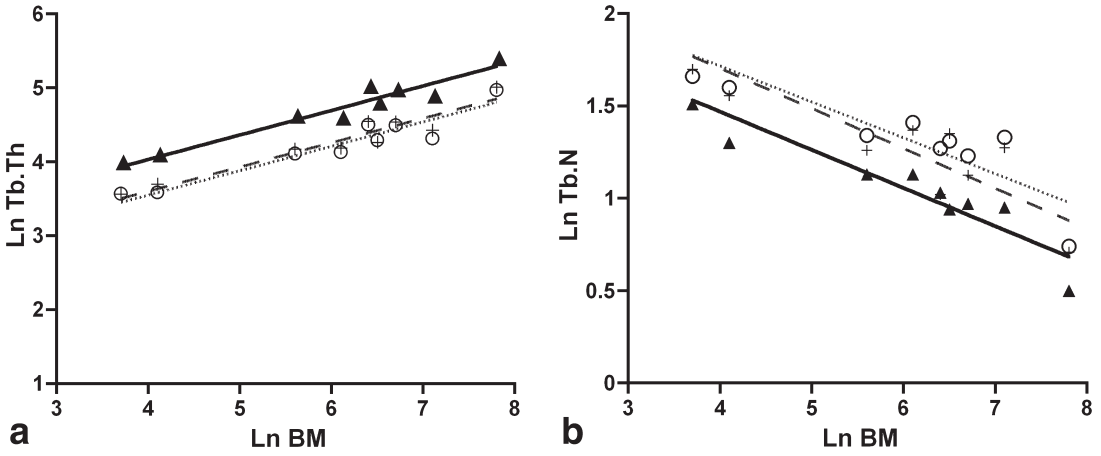

Fig. 5. Trabecular bone architectural scaling patterns for (**a**) trabecular thickness and (**b**) trabecular number. Tb.Th increases with geometric similarity (RMA, b = 0.33, PGLS, b = 0.31) in all three VOI as body mass increases, but Tb.Th values are significantly elevated (P > 0.001) in the vbVOI. Tb.N scales with slight positive allometry in all three VOI (RMA, b =−0.20 to−0.22, PGLS, b =−0.17 to−0.20) but the values are significantly lower (P = 0.001) in the vbVOI. Symbols: ▲, vbVOI, +, crVOI, ○, caVOI.

TABLE 8. Results of the partial correlation analyses of trabecular thickness, body mass, and voxel size

	VbVOI		CrVOI		CaVOI	
Partial r	N = 29	N = 13	N = 29	N = 13	N = 29	N = 13
BM	0.89***	0.56**	0.85***	0.39*	0.84***	0.38*
VOX	0.38***	0.05	0.26**	0.01	0.42***	0.05

BM, body mass, VOX, voxel size. See Table 4 for other abbreviations.* P < 0.05, ** P < 0.01, *** P < 0.001.

(isometry), with individual variability in some species (Fig. 7b,c). The relationship between Ct.BV and Tb.BV was isometric when analyzed with the reduced major axis method: (i) slope = 0.85 (R^2 = 0.94, confidence limits 0.69–1.04, P > 0.001) for species means and (ii) slope = 0.9 (R^2 = 0.68, confidence limits 0.72–1.12, P > 0.001) for individual data. However, PGLS analyses indicated that Tb.BV increased greater than Ct.BV. The slope for this

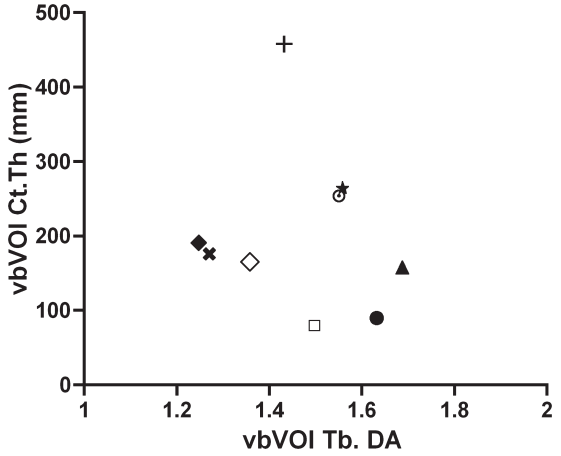

Fig. 6. Cortical shell thickness does not show a clear relationship with Tb.DA.. Symbols: □, *M. rufus*, ●, *M. murinus*, ▲;, *G. senegalensis*, ◇, *C. medius*, ★, *L. leucopus*, ×, *N. coucang*, ⊙, *L. mustelinus*, ◆, *P. potto*, +, *E. macaco.*

regression (Fig. 7b) was 0.79 ($P > 0.001$), the R^2 was 0.93, and the confidence limits of the slope were between 0.64 and 0.95. Finally, total vertebral body bone volume (Ct.BV + Tb.BV) increased isometrically with body mass (Fig. 7d, Tables 6 and 7).

We calculated an index of vertebral body trabecular bone strength in compression that took into account the relative bone mass and the size of the vertebral body (Tb.BV/TV×CSA). The scaling exponent was near 1 and over 90% of the variance in this index could be explained by variation in body mass (Fig. 8).

Mutual Associations

The Tb.BV/TV correlated significantly with several variables (Table 9). Among the trabecular bone structural parameters, numerous measurements (e.g., Tb.Th, Tb.Sp) were significantly correlated (data not shown) but only the Tb.DA was independent of all other measurements (Table 9). These relationships were similar when individual data were analyzed with the RMA method (data not shown).

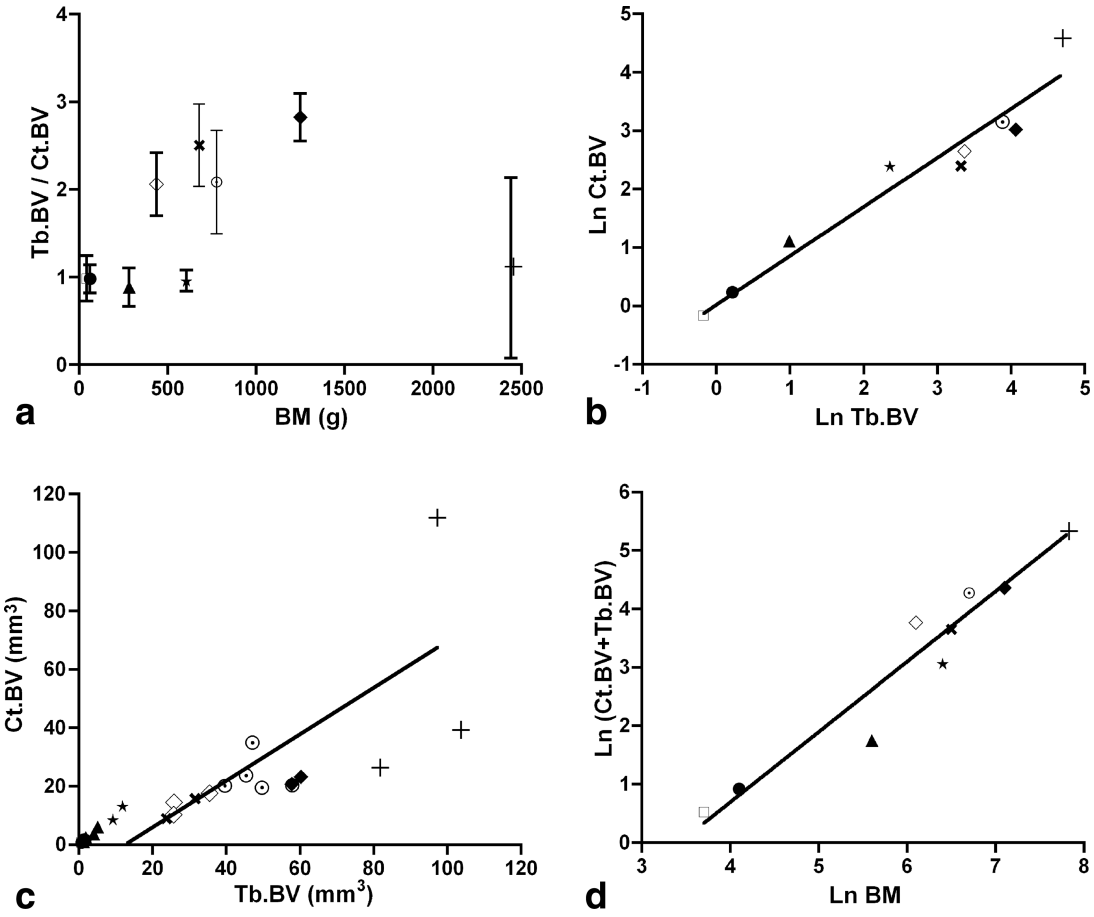

Fig. 7. The ratio of trabecular bone volume to cortical bone volume (**a**) in the last lumbar vertebral body is approximately one in five of the nine species. In two species (*C. medius* and *L. mustelinus*) there is two times more trabecular bone volume compared with cortical bone volume. The ratio reaches 2.5 and 3 in the two lorisines. Scaling exponents are one in RMA analyses when Ct.BV is regressed on Tb.BV (**b** and **c**). PGLS analyses indicate that the scaling exponent is less than one (d), suggesting that Tb.BV increases faster than Ct.BV. The total bone volume in the vertebral body increases isometrically (**d**) in these strepsirhine primates. Symbols: □, *M. rufus*, ●, *M. murinus*, ▲, *G. senegalensis*, ◇, *C. medius*, ★, *L. leucopus*, ×, *N. coucang*, ⊙, *L. mustelinus*, ◆, *P. potto*, +, *E. macaco.*

DISCUSSION

This study of strepsirhine last lumbar vertebral body bone microstructure in small to medium-sized species suggests that many structural variables scale isometrically with body mass. These patterns are generally consistent with macrostructural lumbar vertebral trends identified for strepsirhines (Shapiro and Simons, 2002; Shapiro, 2007) and the fact that this sample consists of a heterogeneous collection of positional behaviors and locomotor modes. Two important parameters to focus on are the Tb.BV/TV and Tb.DA since these two parameters combined can explain up to 90+% of the variance in trabecular bone strength and stiffness (Turner et al., 1990). Relative trabecular bone volumes were similar across the three VOI (Table 4, Fig. 3a). The RMA and PGLS analyses indicated that Tb.BV/TV is not correlated with BM in the vbVOI and caVOI, as predicted by the isometry model. The same analytical approaches indicated that Tb.BV/TV in the crVOI scaled with positive allometry. This trend could not be too strong considering the similarity in Tb.BV/TV values across all VOI. Regardless of the VOI analyzed, there appeared to be two different trends in the data above and below the 600 g to 700 g mark. Specifically, the Tb.BV/TV increased with body mass then plateaued after about 600 g to 700 g. This apparent nonlinear trend is supported by the fact that the Spearman's *rho* values were always higher than the parametric correlations and significant in all three VOI. Pearson's product-moment correlation test is sensitive to linearity while Spearman's correlation test is not (Zar, 1984). It will be interesting to see if this apparent non-linear trend maintains after more species are included to fill in the gaps between 1,200 g and 2,500 g as well as >2,500 g. In comparison with other strepsirhine anatomical sites, femoral head Tb.BV/TV appears to be invariant in strepsirhines (MacLatchy and Müller, 2002; Ryan and Ketcham, 2002). The pattern is unclear in the strepsirhine femoral neck, *G. senegalensis* femoral neck Tb.BV/TV is 45% lower than that in *P. potto* (MacLatchy and Müller, 2002) but no other data are available. It is possible that interspecific BV/TV patterns may be size- and site-dependent within strepsirhines. Trabecular bone volume fraction is likely to have an upper limit because otherwise elements/joints become petrotic and the ability of the trabecular bone to transfer loads decreases and joint health is compromised (Currey, 2002).

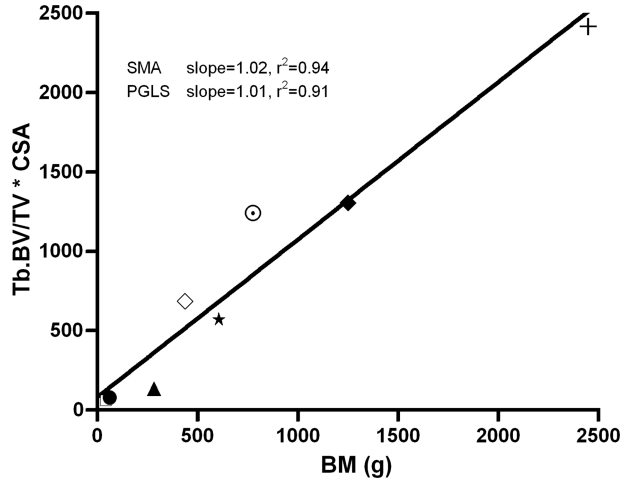

Fig. 8. An index for trabecular bone strength indicates that lumbar vertebral body trabecular bone strength is similar across taxa in this study, relative to body mass. Symbols: □, *M. rufus*, ●, *M. murinus*, ▲, *G. senegalensis*, ◇, *C. medius*, ★, *L. leucopus*, ×, *N. coucang*, ⊙, *L. mustelinus*, ◆, *P. potto*, +, *E. macaco.*

The material fabric (e.g. Tb.DA) is an important correlate of trabecular bone's mechanical properties (Turner et al., 1990) and has been implicated as a correlate of positional behavior in strepsirhine femora (MacLatchy and Müller, 2002; Ryan and Ketcham, 2002). In this study, last lumbar vertebral body Tb.DA appears to be the one truly independent variable; it is not correlated with BM and does not correlate with any other structural parameter. However, Tb.DA appears to contain a positional behavior signal (Fig. 3b). First, the Tb.DA results clearly distinguish *G. senegalensis* and lorisines in our sample, similar to reports for the proximal femur (MacLatchy and Müller, 2002; Ryan and Ketcham,

TABLE 9. Results of mutual associations analyses

	vbVOI		crVOI		caVOI	
	RMA/PGLS	*rho*	RMA/PGLS	*rho*	RMA/PGLS	*rho*
Tb.BV/TV						
Tb.Th	0.83**/0.79*	0.93***	0.86**/0.85**	0.98***	0.76*/0.74*	0.90**
Tb.N	−0.81**/−0.81**	−0.68*	−0.93***/−0.91***	−0.88**	−0.77*/−0.75*	−0.92**
Tb.DA	−0.27/−0.31	−0.12	0.04/−0.21	0.27	0.29/0.22	0.50
Tb.Sp	0.59/0.53	0.82**	–	–	–	–
Tb.SMI	−0.96***/−0.95***	−0.97***	–	–	–	–
Tb.Conn.D	−0.87**/−0.87**	−0.88**	–	–	–	–
CSA	0.60/0.57	0.65	–	–	–	–
Ct.Th	0.72*/0.69*	0.92**	–	–	–	–
Tb.DA						
Tb.Th	−0.25/−0.23	−0.15	0.11/0.07	0.22	0.16/0.12	0.32
Tb.N	0.36/0.29	0.58	−0.20/−0.08	−0.47	−0.11/−0.09	−0.38
Tb.SMI	0.11/0.12	−0.05	–	–	–	–

Correlations test values with Tb.BV/TV and Tb.DA were assessed. Parametric (RMA and PGLS) and nonparametric (*rho*) correlations were determined. See Tables 2 and 5 for explanations.
*$P < 0.05$, **$P < 0.01$, ***$P < 0.001$.

2002). Second, in this data set, the average orthograde, pronograde, and anti-pronograde Tb.DA values decrease, from 1.60 to 1.49 and 1.25, respectively. The anti-pronograde mean Tb.DA is significantly different from the pronograde and orthograde groups. The orthograde mean is also higher than the pronograde average anisotropy value, but the means are not significantly different. This ability to roughly discern positional behaviors with Tb.DA is generally consistent with trends in the strepsirhine femoral head and neck, but stands in contrast to patterns observed in the hominoid thoracic spine (Cotter et al., 2009) and anthropoid proximal femur (Fajardo et al., 2007b; Ryan and Walker, 2010).

Trabecular thickness increased isometrically while Tb.N scaled with positive allometry. This suggests that trabeculae are similar in thickness relative to body size but more numerous at larger and larger body sizes. These scaling relationships were influenced more by body mass changes in the sample than voxel size changes, as demonstrated by the partial correlation results. At present, reconciling these strepsirhine lumbar vertebral body data with other comparative and scaling studies is challenging. Studies vary in trabecular morphometric approaches (three-dimensional direct transformation, two-dimensional plate model, and two-dimensional direct measures), taxonomic samples, target bones, the size variable used to determine allometric equations (femoral head radius, estimated body mass from skeletal dimensions, and published species body mass averages) and scaling results (Mullender et al., 1996; Swartz et al., 1998; Fajardo and Müller, 2001; MacLatchy and Müller, 2002; Ryan and Ketcham, 2002; Fajardo et al., 2007b; Cotter et al., 2009; Ryan and Walker, 2010; Doube et al., 2011). The few studies that have investigated comparative strepsirhine trabecular bone architecture have not assessed the scaling relationships quantitatively. Limited evidence from the strepsirhine femoral head and neck suggested Tb.Th increased from *G. senegalensis* to *P. potto*, with a potentially stronger trend in the femoral neck (MacLatchy and Müller, 2002). The Tb.N decreases from *G. senegalensis* to *P. potto* in the femoral head but the same did not hold for the femoral neck (MacLatchy and Müller, 2002). Several studies of the primate proximal femur (MacLatchy and Müller, 2002; Ryan and Ketcham, 2002; Fajardo et al., 2007; Ryan and Walker, 2010), sampling from different sites therein, and with different approaches, reported invariance of Tb.Th and other parameters with body mass. Recently, Cotter et al. (2009) reported trabecular bone scaling relationships for the eighth thoracic vertebra. They did not directly categorize their results as isometry, positive, or negative allometry, but based on the isometry predictions presented here, those data suggest that Tb.Th scales with negative allometry and Tb.N scales with positive allometry. The apparently slight positive allometry of Tb.N in hominoids matches our result for the strepsirhine spine, while the Tb.Th results are discordant. But Tb.Th negative allometry has been reported for non-volant mammals (Swartz et al., 1998) (using species average data as reported in this study). More recently, that result has been corroborated in a large sample of mammals (Doube et al., 2011). In contrast to the broad mammalian results, Tb.Th scales isometrically and with negative allometry in the femur and humerus of chiropterans (using species average data), respectively (Swartz et al., 1998).

The investigation of trabecular bone scaling is a very new area of study, as evidenced by the few (3) studies that have actually reported empirical scaling results. The discrepancies in reported scaling results may be influenced by numerous factors, including the body size range of the sample, target bone, and its loading mechanics. To begin with, the body size range of the sample appears to impact the scaling relationship of Tb.Th when the results reported here are compared with those for hominoids and mammals. Femoral, humeral, and vertebral trabecular thicknesses consistently scale with negative allometry in broad samplings of nonvolant mammals and in hominoids (Swartz et al., 1998; Cotter et al., 2009; Doube et al., 2011). But in those studies the specimen samples included species with body masses much greater than the strepsirhine species sampled here. If, as recently suggested, trabecular thickness approaches a critical upper limit between 400 and 450 mm, then these strepsirhine data may suggest that while negative allometry describes the broad mammalian scaling pattern for Tb.Th, scaling trends will potentially differ and take on steeper slopes (isometry) at smaller body masses. Swartz et al. (1998) noted that the steeper, relatively isometric slopes among bats appear to reflect patterns visible within the overall nonvolant mammal pattern. This steeper scaling pattern would be possible at small body masses since trabeculae are well below the upper thickness limit and do not threaten the ability of osteocytes to receive nutrients from the marrow cavity via diffusion. In addition to body mass, scaling patterns may be influenced by bone and mechanics. For example, one could envision that trabecular thicknesses and slenderness ratios will scale differently in trabeculae depending on the relative amounts of axial compression versus bending experienced by trabeculae, as might exist between the proximal femur and a lumbar vertebra. The limited number of scaling studies and the poor overlap in taxa and body size also leave open the possibility that the strepsirhine example we report here is unique among primate/mammals. This is an open area for research that will be better understood as more data become available.

We used the direct transformation three-dimensional measurement tools to measure Tb.Th and Tb.N in the vbVOI; this analysis package is nearly ubiquitous among packaged (i.e., hardware and three-dimensional analysis software) μCT systems (e.g., Scanco, GE, SkyScan). We also used the Quant3D analysis package developed by Ketcham and Ryan (Ryan and Ketcham, 2002) in the smaller cranial and caudal spherical VOI. Both of these methods have been validated and used in numerous publications in biomedicine (Rüegsegger et al., 1996; Hildebrand and Rüegsegger, 1997b; Bouxsein et al., 2005; Chappard et al., 2005; Glatt et al., 2007; Buie et al., 2008; Bouxsein et al., 2010; Fajardo et al., 2010) and biological anthropology (Fajardo and Müller, 2001; MacLatchy and Müller, 2002; Ryan and Ketcham, 2002; Ryan and Krovitz, 2006; Fajardo et al., 2007b; Griffin et al., 2010; Wang et al., 2010; DeSilva and Devlin, 2012; Shaw and Ryan, 2012; Wallace et al., 2012). The lower Tb.N values consistently reported in the vbVOI appear to result from architectural variability within the

vertebral bodies. Tb.N visibly decreases in the middle third of all vertebral bodies in Fig. 4 compared with the cranial region, for example. This was confirmed by an analysis of Tb.N in one-third volumes of the vbVOI in all specimens of *M. rufus*, *C. medius*, and *E. macaco* (data not shown). Tb.N was approximately 1.5 times higher in the cranial third of all specimens compared with the middle third region of the trabecular lattice, which was sampled by the vbVOI. In addition, the vbVOI included trabeculae near the endosteal boundary where thicknesses increased as the tissue transitioned to cortical bone. The crVOI and caVOI, on the other hand, sampled trabeculae in the central regions of the cranial- and caudal-most vertebral bodies where trabeculae were much thinner. These site sampling differences most likely drove the uniformly higher Tb.Th values in the vbVOI results.

The Tb.BV/Ct.BV data provide novel insight into the interspecific differences/similarities in the construction of the last lumbar vertebral body. This is a short bone comprised of trabecular bone and a thin cortical shell that work together to give it strength (Biggerman and Brinckman, 1995; Currey, 2002). Assuming compression is the major loading regime in vertebrae (Smit, 2002), the relative bone mass from each structural type would hint at their contributions to bone strength. A few patterns are evident in the ratios of trabecular bone to cortical shell volume. First, there is some interspecific variability in the construction of the vertebral body. The ratio is approximately one in five of the nine species in this sample (Fig. 7a) and that grouping includes pronograde and orthograde taxa. Second, the lorisines have the largest and most homogeneous investment in trabecular bone in the vertebral body compared with all other taxa. Orthograde and pronograde taxa overlap in this ratio. However, it is impossible at this time to determine whether the lorisine ratio is the result of a unique phylogenetic event or due to positional behavior since the lorisines are the only anti-pronograde taxa in the sample. Also, *E. macaco* showed considerable intraspecific variability, so it is unclear if lorisines are unique or *E. macaco*'s result depends more on intraspecific variation in a small sample size. Third, the Tb.BV/Ct.BV generic-level variability of *Lepilemur*, compared with *Microcebus* and the lorisines is striking. *Lepilemur mustelinus* and *L. leucopus* do not show any overlap. Although *Lepilemur* is less dedicated to orthograde postures and vertical clinging than other vertical clinging and leaping strepsirhines, thus far both *Lepilemur* taxa are believed to engage in relatively similar positional behaviors (Nash, 1998; Gebo, 2011). Clearly, further work is necessary to better understand the determinants of strepsirhine lumbar vertebral body construction and its correlation with phylogeny and lumbar mechanics. The differences notwithstanding, it is important to note that the total bone volume of the vertebral body is the same relative to body mass across species (Fig. 7d). Overall, these results suggest some flexibility in the construction of the vertebral body as it pertains to the investment of trabecular bone and cortical bone in the shell.

It will be interesting to investigate further whether *N. coucang*'s and P. *potto's* Tb.BV/Ct.BV ratio is representative of the lorisines. Shell load fraction, or the percent of mechanical load carried by the cortex versus the trabeculae, should decrease as Tb.DA increases because the trabecular bone lattice will be better suited to support the load in conditions of high anisotropy (Silva et al., 1997). In this context, the Tb.DA and Ct.Th should be inversely correlated. Figure 6 shows the relationship between these two variables in our data set, indicating a weak negative trend, at best. A better interspecific test of this hypothesis might assess a full complement of lorisoids or any study sample with a limited spectrum of positional behaviors.

Following the overall trend, CSA scaled isometrically with BM. The scaling coefficient was high (0.80) but the confidence limits included the 0.66 prediction for isometry. Shapiro and Simons (2002) reported a similar finding based on caliper-based measurements of the endplate. Not surprisingly, the term BV/TV$\times$CSA, an index for trabecular bone strength in axial compression, scaled isometrically as well (Fig. 8).

At present, we have only been able to identify minimal evidence for bone mass and architecture changes with increasing body mass that may compensate for the greater loads borne by species of larger size. Vertebral Tb.BV/TV scaled either isometrically or with positive allometry depending on the statistical approach and VOI. In addition, Tb.N scaled with weak positive allometry. These scaling trends may provide sufficient compensation for the greater forces engendered by larger body sizes. However, the fact that the index of vertebral body compressive strength (Tb.BV/TV$\times$CSA) increased isometrically contradicts this interpretation, at least for axial compressive loading conditions. The common pattern of isometry or invariance in our measurements leaves open the question of how vertebral bodies in strepsirhine species compensate for increased body mass.

It is important to note that our study faced some limitations in its ability to address these issues. First, more samples per species will better address the impact of intraspecific variability on our results. As stated earlier, we erred on the side of caution and followed the recommendations of Nunn and Barton (2001) and O'Neill and Dobson (2008) in using species means and phylogenetic statistical methods to examine trabecular scaling patterns and mutual associations among strepsirhines. Although it has not been shown that phylogeny strongly influences trabecular bone architecture, the converse is also true; trabecular bone architecture has not been shown to be independent of phylogeny. Our choice to use species means in our regressions was also driven by the fact that we lacked associated body masses with the majority of these specimens. The impact of species means on regressions is that they do not take into account individual variation. However, the variability in our data, especially for key bone mechanics measurements such as Tb.BV/TV, DA, Ct.Th, and Tb.N are low to modest in magnitude, but others such as Conn.D and Tb.BV appear high. Moreover, levels of variation in our data compare favorably with published data on trabecular bone in strepsirhines (MacLatchy and Müller, 2002; Ryan and Ketcham, 2002). These patterns of intraspecific variation should not be unexpected for typical primate comparative analyses where animals of different ages and sexes are combined. Recognizing this limitation, in several circumstances and where the data and methods allowed, we corroborated our results by

performing analyses on individual data and those results consistently confirmed species means trends. Nevertheless, we recognize that these results need further confirmation using more species and larger sample sizes per species to confirm (or reject) the results we report here. Second, we examined an important load bearing structure in the vertebral column, but we did not analyze features of the posterior processes and zygopophyses, that bear a share of the spinal loads (e.g., extension, Lorenz et al., 1983). As a result, we may have missed an important mechanical signal. Third, we examined the properties of one vertebral level whereas an analysis of different vertebral levels may also shed light on mechanical loading influences on bone morphology. Next, we designed this study to look at scaling patterns across a broad array of strepsirhines. A more focused study targeting related species engaging in a narrower array of positional behaviors might be better designed to assess adaptation in bone to body mass increases. However, we believe the analyses presented here lay the groundwork for just such a study. Lastly, it may very well be the case that discrete analyses of bone variables will have little power to answer the questions we are trying to answer. Discrete analyses do not consistently distinguish locomotor groups at all sites (e.g., proximal femur in anthropoids) and fail to appreciate the synergy between tissue types and different features contributing to bone strength. Ultimately, to better understand whole bone scaling patterns, integrated analyses including trabecular and cortical bone tissues as well as architectures and tissue density will need to be incorporated (e.g., Ryan and Shaw, 2012) to fully understand interspecific relationships between bone and body mass in the vertebral column.

APPENDIX

Below is the phylogeny used in this study, reported in Newick format. (((((mr:8.9,mm:8.9):20.1,cm:29.0):8.0,(ll:1.0,lm:1.0):36.0):5.3,em:42.3):26.2,((nc:35.0,pp:35.0):4.1,gs:39.1):29.4).

ACKNOWLEDGEMENTS

The authors acknowledge the help and generosity of the American Museum of Natural History, the Museum of Comparative Zoology at Harvard University, the Peabody Museum of Comparative Zoology at Yale University, and the University of Zurich. The authors also thank Vahid Entezari for his help with some image analyses. Gabrielle Russo and two anonymous reviewers provided comments that improved the article.

LITERATURE CITED

Biggerman M, Brinckman P. 1995. Biomechanics of osteoporotic fractures. In: Genant HK, Jergas M, van Kujik C, editors. Vertebral fracture in osteoporosis. San Francisco: Radiology Research and Education Foundation. p 21–40.

Bouxsein ML, Boyd SK, Christiansen BA, Guldberg RE, Jepsen KJ, Muller R. 2010. Guidelines for assessment of bone microstructure in rodents using micro-computed tomography. J Bone Miner Res 25:1468–1486.

Bouxsein ML, Myers KS, Shultz KL, Donahue LR, Rosen CJ, Beamer WG. 2005. Ovariectomy-induced bone loss varies among inbred strains of mice. J Bone Miner Res 20:1085–1092.

Buie HR, Moore CP, Boyd SK. 2008. Postpubertal architectural developmental patterns differ between the L3 vertebra and proximal tibia in three inbred strains of mice. J Bone Miner Res 23: 2048–2059.

Chappard D, Retailleau-Gaborit N, Legrand E, Basle MF, Audran M. 2005. Comparison insight bone measurements by histomorphometry and microCT. J Bone Miner Res 20:1177–1184.

Chatterjee HJ, Ho SY, Barnes I, Groves C. 2009. Estimating the phylogeny and divergence times of primates using a supermatrix approach. BMC Evol Biol 9:259.

Chen H, Shoumura S, Emura S, Bunai Y. 2008. Regional variations of vertebral trabecular bone microstructure with age and gender. Osteoporos Int 19:1473–1483.

Cotter MM, Simpson SW, Latimer BM, Hernandez CJ. 2009. Trabecular microarchitecture of hominoid thoracic vertebrae. Anat Rec (Hoboken) 292:1098–1106.

Currey JD. 2002. Bones: structure and mechanics. Princeton, NJ: Princeton University Press.

DeSilva JM, Devlin MJ. 2012. A comparative study of the trabecular bony architecture of the talus in humans, non-human primates, and Australopithecus. J Hum Evol 63:536–551.

Doube M, Klosowski MM, Wiktorowicz-Conroy AM, Hutchinson JR, Shefelbine SJ. 2011. Trabecular bone scales allometrically in mammals and birds. Proc Biol Sci 278:3067–3073.

Eswaran SK, Gupta A, Adams MF, Keaveny TM. 2006. Cortical and trabecular load sharing in the human vertebral body. J Bone Miner Res 21:307–314.

Fajardo RJ, Hernandez E, O'Connor PM. 2007a. Postcranial skeletal pneumaticity: a case study in the use of quantitative microCT to assess vertebral structure in birds. J Anat 211:138–147.

Fajardo RJ, Manoharan RK, Pearsall RS, Davies MV, Marvell T, Monnell TE, Ucran JA, Pearsall AE, Khanzode D, Kumar R, Underwood KW, Roberts B, Seehra J, Bouxsein ML. 2010. Treatment with a soluble receptor for activin improves bone mass and structure in the axial and appendicular skeleton of female cynomolgus macaques (Macaca fascicularis). Bone 46:64–71.

Fajardo RJ, Müller R. 2001. Three-dimensional analysis of nonhuman primate trabecular architecture using micro-computed tomography. Am J Phys Anthropol 115:327–336.

Fajardo RJ, Muller R, Ketcham RA, Colbert M. 2007b. Nonhuman anthropoid primate femoral neck trabecular architecture and its relationship to locomotor mode. Anat Rec 290:422–436.

Fields AJ, Eswaran SK, Jekir MG, Keaveny TM. 2009. Role of trabecular microarchitecture in whole-vertebral body biomechanical behavior. J Bone Miner Res 24:1523–1530.

Gebo DL. 2011. Vertical clinging and leaping revisited: vertical support use as the ancestral condition of strepsirrhine primates. Am J Phys Anthropol 146:323–335.

Glatt V, Canalis E, Stadmeyer L, Bouxsein ML. 2007. Age-related changes in trabecular architecture differ in female and male C57BL/6J mice. J Bone Miner Res 22:1197–1207.

Godfrey L, Sutherland M, Boy D, Gomberg N. 1991. Scaling of limb joint surface areas in anthropoid primates and other mammals. J Zool 223:603–625.

Gong H, Zhang M, Yeung HY, Qin L. 2005. Regional variations in microstructural properties of vertebral trabeculae with aging. J Bone Miner Metabol 23:174–180.

Gosman JH, Ketcham RA. 2009. Patterns in ontogeny of human trabecular bone from SunWatch Village in the prehistoric Ohio Valley: general features of microarchitectural change. Am J Phys Anthropol 138:318–332.

Griffin NL, D'Aout K, Ryan TM, Richmond BG, Ketcham RA, Postnov A. 2010. Comparative forefoot trabecular bone architecture in extant hominids. J Hum Evol 59:202–213.

Guldberg RE, Ballock RT, Boyan BD, Duvall CL, Lin ASP, Nagaraja S, Oest M, Phillips J, Porter BD, Robertson G, Taylor WR. 2003. Analyzing bone, blood vessels, and biomaterials with microcomputed tomography. IEEE Eng Med Biol 22:77–83.

Halloran BP, Ferguson VL, Simske SJ, Burghardt A, Venton LL, Majumdar S. 2002. Changes in bone structure and mass with advancing age in the male C57BL/6J mouse. J Bone Miner Res 17:1044–1050.

Harrigan TP, Jasty M, Mann RW, Harris WH. 1988. Limitations of the continuum assumption in cancellous bone. J Biomech 21: 269–275.

Hernandez CJ, Loomis DA, Cotter MM, Schifle AL, Anderson LC, Elsmore L, Kunos C, Latimer B. 2009. Biomechanical allometry in hominoid thoracic vertebrae. J Hum Evol 56:462–470.

Hildebrand T, Müller R, Laib A, Dequeker J, Rüegsegger P. 1999. Direct three-dimensional morphometric analysis of human cancellous bone: a microstructural data from spine, femur, ilia crest, and calcaneus. J Bone Miner Res 14:1167–1174.

Hildebrand T, Ruegsegger P. 1997a. Quantification of bone microarchitecture with the structure model index. Comput Meth Biomech Biomed Eng 1:15–24.

Hildebrand T, Rüegsegger P. 1997b. A new method for the model-independent assessment of thickness in three-dimensional images. J Microsc 185:67–75.

Ketcham RA, Ryan TM. 2004. Quantification and visualization of anisotropy in trabecular bone. J Microsc 213:158–171.

Laib A, Barou O, Vico L, Lafage-Proust MH, Alexandre C, Rugsegger P. 2000. 3D micro-computed tomography of trabecular and cortical bone architecture with application to a rat model of immobilisation osteoporosis. Med Biol Eng Comput 38:326–332.

Lorenz M, Patwardhan A, Vanderby R, Jr. 1983. Load-bearing characteristics of lumbar facets in normal and surgically altered spinal segments. Spine (Phila Pa 1976) 8:122–130.

MacLatchy L, Müller R. 2002. A comparison of the femoral head and neck trabecular architecture of Galago and Perodicticus using micro-computed tomography (μCT). J Hum Evol 43:89–105.

Maga M, Kappelman J, Ryan TM, Ketcham RA. 2006. Preliminary observations on the calcaneal trabecular microarchitecture of extant large-bodied hominoids. Am J Phys Anthropol 129: 410–417.

Majoral M, Berge C, Casinos A, Jouffroy FK. 1997. The length of the vertebral column of primates: An allometric study. Folia Primatol 68:57–76.

Martins EP, Hansen TF. 1997. Phylogenies and the comparative method: a general approach to incorporating phylogenetic information into the analysis of interspecific data. Am Nat 149: 646–667.

Masters JC, Boniotto M, Crovella S, Roos C, Pozzi L, Delpero M. 2007. Phylogenetic relationships among the Lorisoidea as indicated by craniodental morphology and mitochondrial sequence data. Am J Primatol 69:6–15.

Matsui A, Rakotondraparany F, Munechika I, Hasegawa M, Horai S. 2009. Molecular phylogeny and evolution of prosimians based on complete sequences of mitochondrial DNAs. Gene 441:53–66.

McBroom RJ, Hayes WC, Edwards WT, Goldberg RP, White AA, 3rd. 1985. Prediction of vertebral body compressive fracture using quantitative computed tomography. J Bone Joint Surg Am 67: 1206–1214.

Meinel L, Fajardo R, Hofmann S, Langer R, Chen J, Snyder B, Vunjak-Novakovic G, Kaplan D. 2005. Silk implants for the healing of critical size bone defects. Bone 37:688–698.

Mullender MG, Huiskes R, Versleyen H, Buma P. 1996. Osteocyte density and histomorphometric parameters in cancellous bone of the proximal femur in five mammalian species. J Orthop Res 14: 972–979.

Müller R, Koller B, Hildebrand T, Laib A, Gionollini S, Rüegsegger P. 1996. Resolution dependency of microstructural properties of cancellous bone based on three-dimensional μ-tomography. Technol Health Care 4:113–119.

Nash L. 1998. Vertical clingers and sleepers: seasonal influences on the activities and substrate use of Lepilemur leucopus at Besa Mahafly Special Reserve. Madagascar. Folia Primatol 69:204–217.

Nunn CL, Barton RA. 2001. Comparative methods for studying primate adaptation and allometry. Evol Anthropol 10:81–98.

O'Neill MC, Dobson SD. 2008. The degree and pattern of phylogenetic signal in primate long-bone structure. J Hum Evol 54: 309–322.

Parfitt AM, Mathews CHE, Villanueva AR, Kleerekoper M, Frame B, Rao DS. 1983. Relationships between surface, volume, and thickness of iliac trabecular bone in aging and osteoporosis. J Clin Invest 72:1396–1409.

Parsons T, Ryan TM, Reeves RH, Richtsmeier JT. 2007. Microstructure of trabecular bone in a mouse model for Down syndrome. Anat Rec (Hoboken) 290:414–421.

Purvis A. 1995. A composite estimate of primate phylogeny. Phil Trans R Soc Lond B 348:405–421.

Ridler TW, Calvard S. 1978. Picture thresholding using an iterative selection method. IEEE Trans Syst Man Cybernet SMC 8: 630–632.

Rockoff SD, Sweet E, Bleustein J. 1969. The relative contribution of trabecular and cortical bone to the strength of human lumbar vertebrae. Calcif Tissue Res 3:163–175.

Rüegsegger P, Koller B, Müller R. 1996. A microtomographic system for the nondestructive evaluation of bone architecture. Calcif Tissue Res 58:24–29.

Ryan TM, Ketcham RA. 2002. The three-dimensional structure of trabecular bone in the femoral head of strepsirhine primates. J Hum Evol 43:1–26.

Ryan TM, Krovitz GE. 2006. Trabecular bone ontogeny in the human proximal femur. J Hum Evol 51:591–602.

Ryan TM, Shaw CN. 2012. Unique suites of trabecular bone features characterize locomotor behavior in human and non-human anthropoid primates. PloS one 7:e41037.

Ryan TM, Walker A. 2010. Trabecular bone structure in the humeral and femoral heads of anthropoid primates. Anat Rec (Hoboken) 293:719–729.

Seiffert ER. 2007. Early evolution and biogeography of lorisiform strepsirrhines. Am J Primatol 69:27–35.

Seiffert ER, Simons EL, Attia Y. 2003. Fossil evidence for an ancient divergence of lorises and galagos. Nature 422:421–424.

Shapiro LJ. 2007. Morphological and functional differentiation in the lumbar spine of lorisids and galagids. Am J Primatol 69: 86–102.

Shapiro LJ, Seiffert CVM, Godfrey LR, Jungers WL, Simons EL, Randria GFN. 2005. Morphometric analysis of lumbar vertebrae in extinct Malagasy strepsirrhines. Am J Phys Anthropol 128: 823–839.

Shapiro LJ, Simons CVM. 2002. Functional aspects of strepsirrhine lumbar vertebral bodies and spinous processes. J Hum Evol 42: 753–783.

Shaw CN, Ryan TM. 2012. Does skeletal anatomy reflect adaptation to locomotor patterns? Cortical and trabecular architecture in human and nonhuman anthropoids. Am J Phys Anthropol 147: 187–200.

Silva MJ, Keaveny TM, Hayes WC. 1997. Load sharing between the shell and centrum in the lumbar vertebral body. Spine 22: 140–150.

Smit TH. 2002. The use of a quadruped as an in vivo model for the study of the spine - biomechanical considerations. Eur Spine J 11: 137–144.

Smith RJ, Cheverud JM. 2002. Scaling of sexual dimorphism in body mass: a phylogenetic analysis of Rensch's rule in primates. Int J Primatol 23:1095–1135.

Smith RJ, Jungers WL. 1997. Body mass in comparative primatology. J Hum Evol 32:523–559.

Swartz SM, Parker A, Huo C. 1998. Theoretical and empirical scaling patterns and topological homology in bone trabeculae. J Exp Biol 201:573–590.

Trussell HJ. 1979. Comments on "picture thresholding using an iterative selection method". IEEE Trans Syst Man Cybernet SMC 9:311.

Turner CH. 1992. On Wolff's Law of trabecular architecture. J Biomech 25:1–9.

Turner CH, Cowin SC, Rho JY, Ashman RB, Rice JC. 1990. The fabric dependence of the orthotropic elastic constants of cancellous bone. J Biomech 23:549–561.

Underwood EE. 1970. Quantitative stereology. Reading, MA: Addison-Wesley Publishing Co.

Wallace IJ, Tommasini SM, Judex S, Garland T, Jr., Demes B. 2012. Genetic variations and physical activity as determinants of limb

bone morphology: an experimental approach using a mouse model. Am J Phys Anthropol 148:24–35.
Wang Q, Ashley DW, Dechow PC. 2010. Regional, ontogenetic, and sex-related variations in elastic properties of cortical bone in baboon mandibles. Am J Phys Anthropol 141: 526–549.
Warton DI, Weber NC. 2002. Common slope tests for bivariate errors-in-variables models. Biom J 44:161–174.
Warton DI, Wright IJ, Falster DS, Westoby M. 2006. Bivariate line-fitting methods for allometry. Biol Rev 81:259–291
Weibel ER. 1979. Stereological methods. New York: Academic Press.
Weibel ER. 1980. Stereological methods. New York: Academic Press.
Yoder AD, Yang Z. 2004. Divergence dates for Malagasy lemurs estimated from multiple gene loci: geological and evolutionary context. Mol Ecol 13:757–773.
Yoganandan N, Myklebust JB, Cusick JF, Wilson CR, Sances A. 1988. Functional biomechanics of the thoracolumbar vertebral cortex. Clin Biomech 3:11–18.
Zar JH. 1984. Biostatistical analysis. Englewood Cliffs, NJ: Prentice-Hall.